

Intra-Burst Interaction During Ultrashort Pulsed Laser Structuring of Metals with Variable Temporal Pulse Spacing

Benedikt Bornschlegel¹ and Dennis Haasler^{*2}

¹Chair for Laser Technology LLT – RWTH Aachen University,
Steinbachstr. 15, 52074 Aachen, Germany

²Fraunhofer Institute for Laser Technology ILT,
Steinbachstr. 15, 52074 Aachen, Germany

*Corresponding author's e-mail: benedikt.bornschlegel@llt.rwth-aachen.de

One approach to increase productivity of ultrashort pulse laser processing is the use of pulse bursts. The small temporal spacing between the pulses within a burst results in an increasing influence of intra-burst heat accumulation, shielding effects and redeposition of ablated material. Even an increase in ablation efficiency can be achieved by bursts. To gain a deeper understanding of these effects, burst ablation with flexible intra-burst pulse spacing is investigated. The industrial relevant materials copper, aluminum and stainless steel are compared regarding their dominating effects based on the pulse ablation efficiency. Surface effects and the ablation quality achieved are evaluated by means of the surface roughness. The time periods of the secondary effects redeposition, shielding and amplified ablation are identified and discussed for all three materials. Thus, a great potential for highly efficient tailored burst processes by adjusting the temporal pulse spacings is shown.

DOI: 10.2961/jlmn.2024.01.2009

Keywords: ultrashort, USP, ablation, burst, structuring, metal, shielding, redeposition, ultrafast

1. Introduction

Ultrashort pulse (USP) laser metal processing is characterized by its high precision, versatility and quality compared to longer pulsed laser processing [1–3]. However, due to the low achievable ablation rate and therefore comparably lower productivity, USP processing has only been established in specific industrial sectors so far [4–6]. Therefore, the implementation of ultrafast laser systems with average powers in the range of hundreds of Watts is an important USP research topic since several years [4,7–13]. Also, the upscaling of USP processes is not trivial as the most efficient operating point is about e^2 -times the material specific ablation threshold [9,14]. Scaling approaches therefore cannot consist of a simple increase of the pulse energy.

Different approaches are being investigated to overcome this limitation. Three promising concepts to apply a high average power effectively are: the utilization of high repetition rates [4,12,15], the process parallelization via multi beam optical systems [11,16–19] and the use of pulse bursts [6,20–30]. Using high repetition rates requires complex system engineering such as polygon scanners to realize a beam deflection fast enough to realize the pulse separation necessary to control arising heat accumulation and shielding effects [4,10]. The multi beam concept also requires specific optical systems and system technology and elaborate process design due to amplified heat accumulation by adjacent beamlets [16,19]. With both approaches the user loses some degrees of freedom and thus flexibility in terms of process design and applicability. The only approach which does not require specific optical or deflection systems and can be implemented with conventional scanner systems is the application of pulse bursts. Therefore, it is the most universal approach

and can be implemented on existing laser machining systems. In this approach the single pulses of the USP-process are replaced with pulse bursts with the laser seeder frequency. Typical seeder frequencies are in the range of tens of megahertz and lead to a small temporal separation between the pulses, which results in an high influence of intra-burst heat accumulation and shielding effects. The achieved quality [31] and efficiency [23] of the burst processes can be significantly affected by these secondary effects. Even an increase in the ablation efficiency is possible for specific burst configurations and some materials [6,23,32,33]. Disabled shielding, ablation of molten material and an increased absorption are discussed as cause of this “amplified ablation”. The heat accumulation can lead to smoother surface finishings due to melting but always affects the achievable precision. Shielding effects reduce the effective pulse energy at the material surface by absorption, scattering or reflection in the ablation products. Therefore, the achievable process efficiency decreases. Furthermore, an alternating efficiency dependent on the number of pulses per burst has been reported for copper many times, which is still not fully understood [6,20,21,23,28,32–36]. This effect is reported for bursts in the MHz regime and is therefore probably dependent on temporal pulse spacings. Also the hypothesis of material redeposition by the even numbered pulses in the burst is postulated [23,32,35]. To distinguish between shielding and redeposition is challenging since redeposition always implies shielding. In an ex-situ evaluation, as by comparing ablation efficiencies, redeposition can only be determined if the efficiency contribution of a pulse becomes negative. To achieve a deeper understanding of the shielding and redeposition and the temporal regimes of these effects, burst

ablation with flexible pulse spacing is investigated. The industrial relevant materials copper, aluminum and stainless steel are compared regarding their dominating effects based on the ablation efficiency. For the targeted investigation of the occurring secondary effects experiments with increasing number of pulses per burst are carried out. The flexible bursts provided by the used beam source allow the variation of the temporal pulse spacing between the last two pulses within the burst. Thus, the pulse specific efficiency is evaluated regarding redeposition, shielding and amplified ablation.

2. Experimental setup and procedure

For experimental investigation of the secondary effects occurring during burst processing two high power ultrashort pulsed laser systems FX600 and FX400 from Edge-Wave GmbH are used. Both laser sources allow to disable arbitrary pulses within a burst of up to 16 pulses. Therefore, temporal flexible bursts with a pulse spacing of n times the seeder pulse interval of 20 ns are enabled. For focusing and deflection of the laser beam an excelliSCAN14 from SCANLAB GmbH with a 160 mm f-theta optic from JENOPTIK AG is utilized. For comparison of the ablation efficiency cavities with dimensions of $3 \times 3 \text{ mm}^2$ are machined on the sample surface. The scan strategy is a bidirectional line scan with burst overlap BO and line overlap LO of $\sim 75 \%$ and rotated by 90° with each layer for a homogeneous ablation as schematically shown in Fig. 1. The burst overlap is hereby defined as the distance between the first pulse of two consecutive bursts, the intra-burst pulse distance is neglected. The number of scanned layers is estimated by the material specific expected efficiency and a target ablation depth. The burst repetition rate f_{rep} is set to 300 kHz since it's the highest repetition rate which provides the maximum pulse energy for these laser systems. This is necessary because the pulse energy is split up into bursts. For all presented experiments the remaining essential process parameters are kept constant and are listed in Table 1. The three industrial relevant metals copper, aluminum and stainless steel are investigated. The following abbreviations assigned to the materials are used: copper (CW024A) *Cu*, aluminum (AW-5005A) *Al* and stainless steel (1.4301) *StSt*.

Table 1 Summary of the used process parameters.

Process parameter		
Wavelength	λ	1030 nm
Focus diameter	$2w_0$	32 – 42 μm
Pulse duration	τ	1.5 ps
Pulse per Burst	PpB	1 – 4 PpB
Burst overlap	BO	$\sim 75 \%$
Line overlap	LO	$\sim 75 \%$
Burst repetition rate	f_{rep}	300 kHz
Pulse repetition rate	f_{secd}	50 MHz
Single pulse peak fluence	F_0	0.8/1.9/4.8 J/cm ² *

*depending on the material type

For the measurement of the ablation depth and the resulting surface a Keyence VR5200 Profilometer and Keyence VK-X3000 Laser Scanning Microscope is used respectively. The data evaluation is performed with the MountainsMap software from Digital Surf SARL.

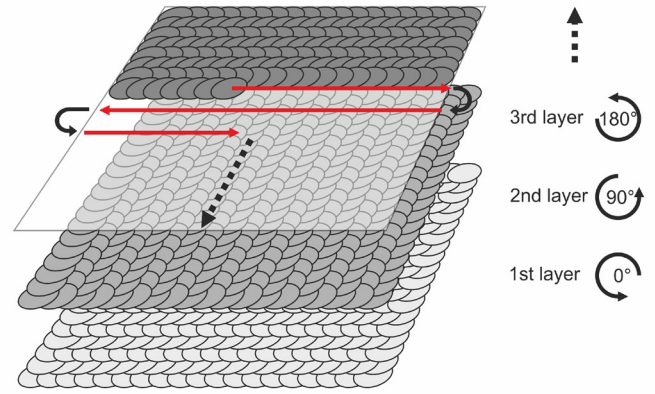


Fig. 1 Cavity scan strategy for ablation efficiency study.

For a more descriptive presentation and intuitive interpretation of the data and the impact of secondary effects, the measured process ablation efficiency is converted into a pulse ablation efficiency. Referred to in the following as process efficiency and pulse efficiency. It is assumed, that the pulse efficiencies determined for n pulses per burst (PpB) remain the same for $n+1$ PpB and the $n+1$ pulse efficiency can be calculated with equation 1. For example, the efficiency of the second pulse within a burst with two pulses can be determined, if the efficiency of the first pulse is known from a single pulse process.

$$\varepsilon_{\text{pulse } n} = n \cdot \varepsilon_{\text{burst } n} - \sum_{i=1}^{n-1} \varepsilon_i \quad (1)$$

Using equation 1 the ablation efficiency $\varepsilon_{\text{pulse } n}$ of the last pulse within a burst can be calculated, if the $n-1$ pulse efficiencies are known. Where n is the number of pulses per burst, $\varepsilon_{\text{burst } n}$ is the burst process efficiency and ε_i the ablation efficiency of the i -th pulse. By successively increasing the number of pulses per burst step by step, the efficiency of the last pulse in the burst can be calculated iteratively. With this method the pulse efficiencies of the second, third and fourth pulse of up to four pulses per burst are calculated in section 3.

3. Experimental results

In the following section the efficiency and surface roughness of time equidistant bursts (as reference) and of time flexible bursts are presented. For better comparability the efficiency of the last pulse of a burst is calculated for the flexible bursts as described in section 2.

Fig. 2 shows the equidistant reference processes for copper (Cu), aluminum (Al) and stainless steel (StSt). For all processes the optimum single pulse peak fluence of the respective material is used. The mentioned alternating efficiency is visible for copper and aluminum for up to 6 PpB. For an even number of pulses within a burst, the efficiency drops significantly compared to the previous number of pulses. For 7 PpB and above heat accumulation dominates the process for stainless steel and leads to a molten surface finish and low Sa values (cf. Fig. 3). This heat accumulation is also present for aluminum and copper but in this case results in a rough surface finish (cf. Fig. 3 and Fig. 4 c)), which leads to higher absorption and thus higher ablation efficiencies. For stainless steel no alternating efficiency can be

observed. For copper and aluminum and 2 PpB, the efficiency drops below 50 % of the single pulse efficiency. This means the second pulse redeposits ablation products of the first pulse instead of removing material. This leads to a negative pulse efficiency, as seen in Fig. 5 for the second pulse at 20 ns temporal separation. Therefore, the absolute material removal rate of this process is less compared to the single pulse process.

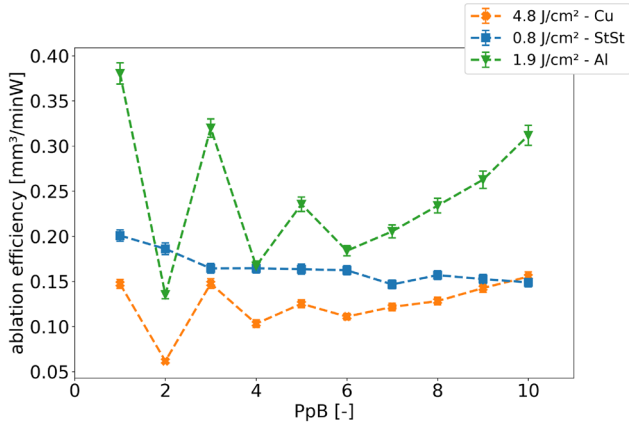


Fig. 2 Ablation efficiency for the material specific optimum single pulse fluence over number of pulses per burst. For copper and aluminum an alternating efficiency effect can be observe for up to 6 PpB.

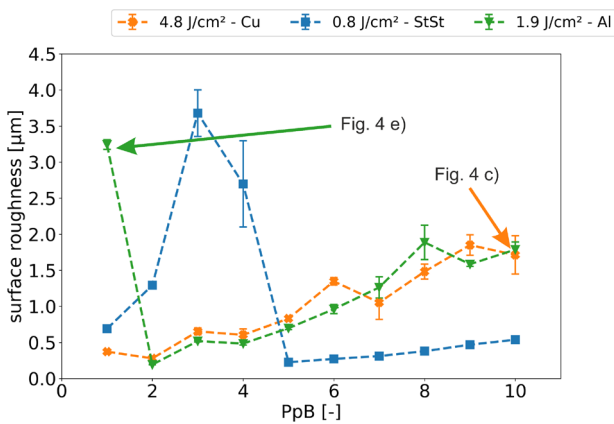


Fig. 3 Surface roughness for the material specific optimum single pulse fluence as a function of number of pulses per burst. For aluminum and stainless steel, surface effects increase the roughness for specific parameter settings.

The surface roughness is rising with increasing pulses per burst due to higher ablation volumes per burst and greater intra-burst heat accumulation. The only exceptions to this are 1 PpB for aluminum and 1 – 4 PpB for stainless steel. For aluminum the formation of local areas with micro hole formation arises (cf. Fig. 3). Stainless steel in contrast shows wavy self-organized line structures for 2 - 4 PpB which originate from melting Cone Like Protrusions. The occurrence of self-organizing microstructures such as LIPSS (laser-induced periodic surface structures) and CLP (Cone-Like Protrusion [37] cf. Fig. 4 a)) are known for USP metal processing, but the underlying causes are not yet fully understood. The interaction of plasmonic and thermal effects are suspected as most probable cause which are impaired by increasing heat accumulation. Furthermore, the formation of such structures during burst processing as a function of the

fluence and number of pulses in the burst similar to the behavior of stainless steel (cf. Fig. 3) is reported by Brenner et al. [38,39].

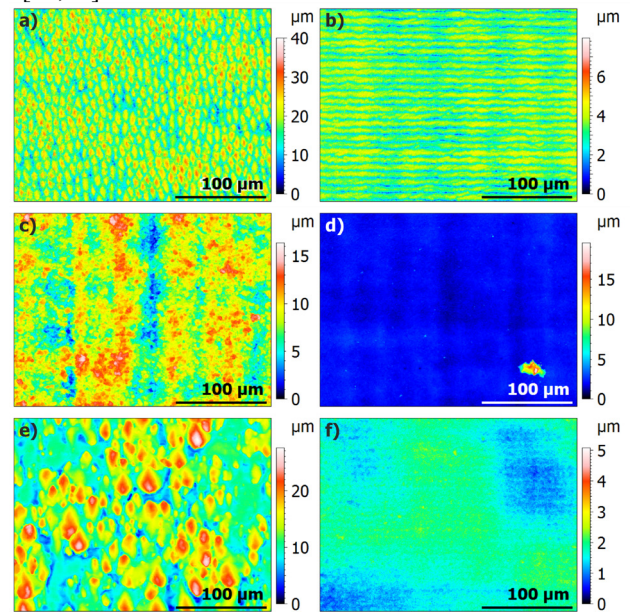


Fig. 4 LSM images of surface conditions for rough and smooth finishes for stainless steel (a, b), copper (c, d) and aluminum (e, f).

In the following the efficiency for bursts with flexible temporal spacings is evaluated. For these experiments the temporal distance between the last two pulses of a bursts is varied. The number of pulses per burst is hereby increased from 2 to 4 PpB. In Fig. 5 the efficiency of the second pulse in a burst with two pulses is plotted as a function of the temporal spacing Δt_1 between the first and the second pulse. The efficiency of the first pulse is shown as a reference line for all three materials. The temporal spacing between the first and the second pulse Δt_1 is varied from 20 to 300 ns. For stainless steel only for 20 ns a shielding effect becomes noticeable by a drop in the efficiency. For temporal spacings longer than 40 ns no significant efficiency reduction is evident. Copper and aluminum ablation with 20 ns temporal spacing both result in a negative pulse efficiency which indicates a redeposition of ablated material by the second pulse. For copper, the efficiency is below the single pulse efficiency for up to 160 ns. During this time frame shielding of the second pulse by ablation products of the first pulse takes place, which are still present above the ablated surface. For a temporal separation above 160 ns the second pulse ablates as efficient as the first pulse. Even a slight increase can be seen. Therefore, the shielding effect vanishes for a time regime greater than 160 ns. For aluminum, shielding of the second pulse continues until a temporal separation of approximately 300 ns and may still be present in this regime.

The resulting surface roughnesses for the 2 PpB experiments with increasing Δt_1 are shown in Fig. 6. The dashed lines indicate the surface roughness of the corresponding single pulse processes. For stainless steel and $\Delta t_1 = 20$ ns, wavy line structures are visible but are smoothed with increasing temporal spacing and becomes a straight line structure with a period of approximately 8 μm which corresponds with the line overlap LO used in this case (cf. Fig. 4 b)). Copper shows a slight increase in its roughness with increasing efficiency and therefore higher ablation volume per burst.

Aluminum also shows an increase in roughness with increasing ablation volume but shows simultaneously the development of isolated micro hole formations. In both cases the efficiency increases with larger temporal pulse spacing and therefore also the roughness.

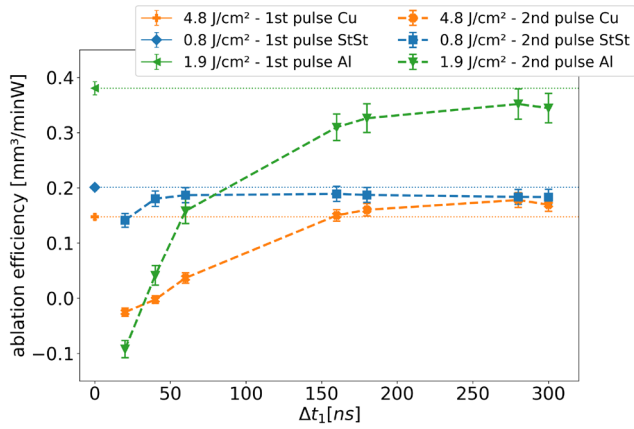


Fig. 5 Ablation efficiency of the second pulse in a burst with two pulses as a function of increasing pulse spacing Δt_1 .

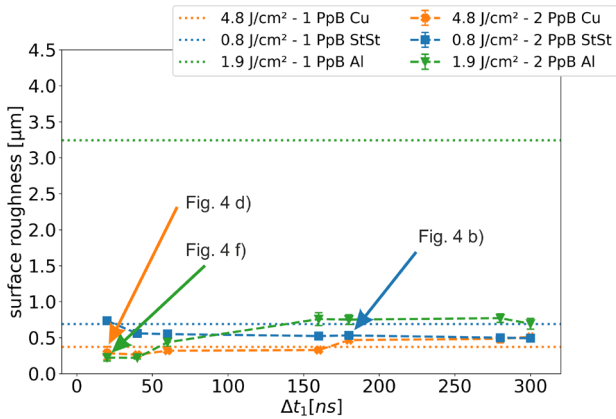


Fig. 6 Surface roughness after an ablation process with two pulses per burst as a function of the temporal pulse spacing

In Fig. 7 the pulse efficiency for different temporal spacings is shown for a burst with 3 PpB. The temporal spacing between the first and second pulse is kept constant with $\Delta t_1 = 20$ ns and Δt_3 between the second and third pulse is varied. Thus, the pulse efficiency can be calculated by using the efficiency of the second pulse for 2 PpB and $\Delta t_1 = 20$ ns. For stainless steel, a drop of efficiency for 40 ns to approximately 120 ns becomes visible. However, for shorter temporal spacings than 40 ns the efficiency increases again. This may show a relevant shielding effect of the third pulse which is overcompensated by intra-burst heat accumulation for $\Delta t_1 = \Delta t_2 = 20$ ns. For $\Delta t_2 \geq 140$ ns, an efficiency slightly above the single pulse process is calculated for the third pulse. This can be explained by a neglectable shielding effect and a still relevant intra-burst heat accumulation. For copper, the third pulse shows a pulse efficiency above the first pulse for all investigated temporal spacings. This indicates a more efficient ablation of the redeposited material of the second pulse. For 20 ns, the pulse efficiency of the third pulse is more than doubled compared to the first pulse with a drop to values around 0.2 mm³/min/W for longer temporal spacings. Aluminum also shows amplified ablation for all

temporal spacings up to 280 ns with a steady drop in efficiency with an increasing spacing. The dependence of the amplified ablation on the temporal spacing could be due to heat conduction. The hot and partly liquid ablation products pushed back into the ablation crater could be responsible for the amplified ablation due to increase absorption. But due to the small amount of redeposited material, rapid cooling takes place. Furthermore, sintering of the particles to the sample surface could also accompany the cooling process.

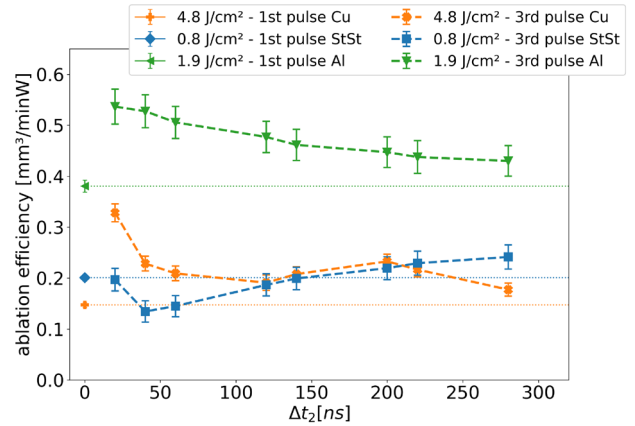


Fig. 7 Ablation efficiency of the third pulse in a burst with three pulses with increasing pulse spacing Δt_2 .

Fig. 8 shows the surface roughness for the ablation with 3 PpB and flexible temporal spacing Δt_2 . For copper and aluminum no significant changes in the surface condition become evident with increasing pulse spacing. Only an increased occurrence of particles on the sample surface becomes visible for copper. Stainless steel in contrast enters a CLP regime for 3 PpB. For $\Delta t_2 = 40$ ns, the CLP formation covers the whole processed area (cf. Fig. 8) but decreases in spatial height with increasing temporal spacing and switches to a wavy line structure for long spacings which originates from molten CLP structures.

Fig. 9 shows the ablation efficiency of the fourth pulse of 4 PpB with $\Delta t_1 = \Delta t_2 = 20$ ns as a function of the variation of Δt_3 between the third and fourth pulse. For stainless steel, a similar behavior compared to 3 PpB can be observed. A shielding effect for the fourth pulse is present for up to approximately 120 ns. After this, the pulse efficiency is comparable to the efficiency of the first pulse. For short temporal spacings the ablation efficiency of copper and aluminum is similar to 2 PpB respectively, because for 20 ns a negative pulse efficiency indicates redeposition of material with the fourth pulse. For approximately up to 100 ns for both materials shielding of the fourth pulse is still relevant but for larger temporal spacings the ablation behavior changes compared to 2 PpB. In the case of 4 PpB, the pulse efficiency of the fourth pulse exceeds that of the single pulse ablation and indicates therefore an amplified ablation for aluminum and copper. Thus, this represents a temporal regime for highly efficient ablation of copper and aluminum with process efficiencies exceeding those of 1, 2 and 3 PpB.

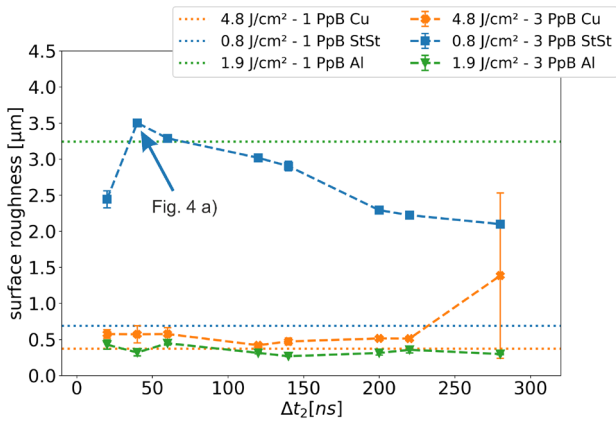


Fig. 8 Surface roughness after an ablation process with three pulses per burst as a function of the temporal pulse spacing of the third pulse.

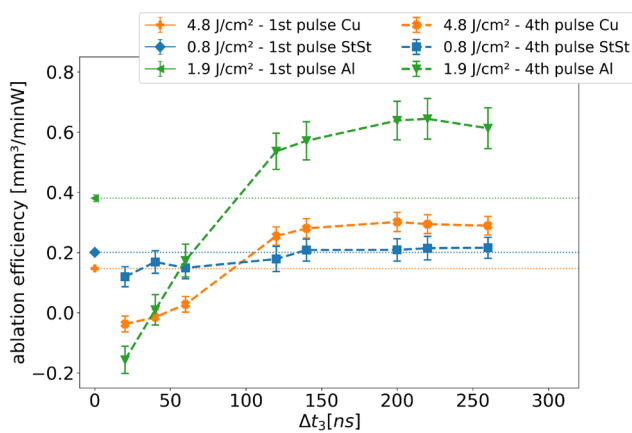


Fig. 9 Ablation efficiency of the fourth pulse in a burst with four pulses as a function of increasing pulse spacing Δt_3 .

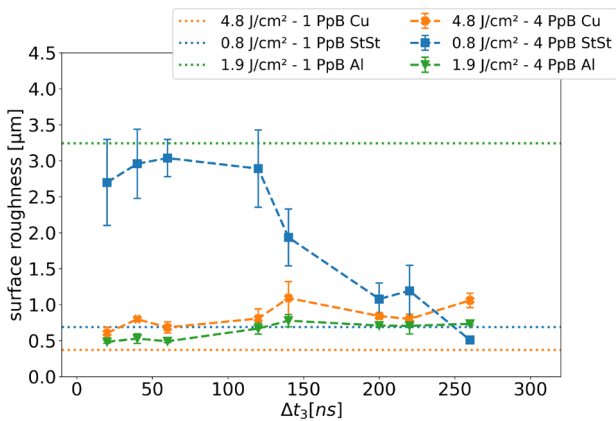


Fig. 10 Surface roughness after an ablation process with four pulses per burst as a function of the temporal pulse spacing.

For 4 PpB the surface roughness is plotted in Fig. 10 and shows an offset compared to 1 PpB and a slight increase of roughness with the temporal pulse spacing for copper and aluminum. This is attributable to the higher ablation volume per burst. The increased ablation volume is also represented by more particles covering the processes sample surface as the removal of the particles via a suction system becomes challenging with increasing removal rates. For stainless steel a transitional regime becomes visible where melt is created because of the heat accumulation which begins to cover the

CLP patterns. This leads to a polishing effect for the surface finish of the processes with a large Δt_3 , as shielding is not present the full pulse energy is coupled into the material.

4. Conclusion

In this work the influence of the temporal pulse spacing on the ablation efficiency and surface roughness of ultra-short pulsed burst processes is investigated. As sample material three industrial relevant metals are chosen: copper, aluminum and stainless steel. The identified time periods of the secondary effects redeposition, shielding and amplified ablation are summarized in Table 2. The most important findings presented in this work are summarized in the following.

Table 2 Summary of the time periods of the secondary effects.

		Redeposition	Shielding	Amplified Ablation
2nd pulse of 2 PpB $\Delta t_1 = X$	Cu	$\Delta t_1 = 20 \text{ ns}$	$\Delta t_1 < 160 \text{ ns}$	-
	StSt	-	$\Delta t_1 = 20 \text{ ns}$	-
	Al	$\Delta t_1 = 20 \text{ ns}$	$\Delta t_1 \leq 300 \text{ ns}$	-
3rd pulse of 3 PpB $\Delta t_1 = 20 \text{ ns}$ $\Delta t_2 = X$	Cu	-	-	$\Delta t_2 \leq 300 \text{ ns}$
	StSt	-	$\Delta t_2 \leq 120 \text{ ns}$	-
	Al	-	-	$\Delta t_2 \leq 300 \text{ ns}$
4th pulse of 4 PpB $\Delta t_1 = \Delta t_2 = 20 \text{ ns}$ $\Delta t_3 = X$	Cu	$\Delta t_3 = 20 \text{ ns}$	$\Delta t_3 < 100 \text{ ns}$	$300 \text{ ns} \geq \Delta t_3 > 100 \text{ ns}$
	StSt	-	$\Delta t_3 \leq 120 \text{ ns}$	-
	Al	$\Delta t_3 = 20 \text{ ns}$	$\Delta t_3 < 100 \text{ ns}$	$300 \text{ ns} \geq \Delta t_3 > 100 \text{ ns}$

For copper, the dropping ablation efficiency for even number of pulses in a burst is known. Here it is shown, that for the second pulse of 2 PpB shielding and redeposition ends with approximately 160 ns pulse spacing and the full process efficiency is recovered. For the fourth pulse of 4 PpB, redeposition and shielding already ends after approximately 120 ns and even an amplified ablation is observed for longer temporal spacings. For the third pulse of 3 PpB, the known amplified ablation is present for all studied pulse spacings. Aluminum shows a very similar behavior compared to copper regarding the intra-burst interaction. Only the explicit time periods of the regimes differ and melt and self-organized surface effects occur in specific constellations, which show parallels to the behavior of stainless steel. In contrast to this, for stainless steel only shielding and heat accumulation seems to be relevant intra-burst interactions. Shielding is occurring up to 120 ns according to the efficiency drop, but intra-burst heat accumulation may over-compensate some of the shielding at short temporal spacings due to the low thermal conductivity.

A great potential is shown in this work to tailor burst processes by adjusting the temporal spacings of single pulses in the burst for highly efficient copper and aluminum ablation. Even for stainless steel some adjustments can be beneficial because surface effects impairing the quality and precision can be avoided while keeping the applied average power high. In further experiments, the time periods of the different secondary effects are to be examined regarding the applied fluence per pulse. Furthermore, tailored burst processes are currently developed and investigated for all three materials.

Acknowledgments

This research is funded by the Digital Photonic Production DPP Research Campus as part of the "Research Campus Public-Private Partnership for Innovation" research funding initiative of the German Federal Ministry of Education and Research (BMBF). As part of the German government's high-tech strategy, the BMBF is using this initiative to promote strategic and long-term cooperation between science and industry "under one roof". (Funding number: 13N15423)

References

- [1] S. Nolte, C. Momma, H. Jacobs, A. Tünnermann, B. N. Chichkov, B. Wellegehausen, and H. Welling: *J. Opt. Soc. Am. B*, 14, (1997) 2716.
- [2] C. Momma, B. N. Chichkov, S. Nolte, F. von Alvensleben, A. Tünnermann, H. Welling, and B. Wellegehausen: *Opt. Commun.*, 129, (1996) 134.
- [3] B. N. Chichkov, C. Momma, S. Nolte, F. Alvensleben, and A. Tünnermann: *Appl. Phys. A*, 63, (1996) 109.
- [4] J. Schille, L. Schneider, A. Streek, S. Kloetzer, and U. Loeschner: *Opt. Eng.*, 55, (2016) 96109.
- [5] J. Finger and M. Reininghaus: *Opt. express*, 22, (2014) 18790.
- [6] T. Kramer, B. Neuenschwander, B. Jäggi, S. Remund, U. Hunziker, and J. Zürcher: *Phys. Procedia*, 83, (2016) 123.
- [7] A. Ancona, S. Döring, C. Jauregui, F. Röser, J. Limpert, S. Nolte, and A. Tünnermann: *Opt. Lett.*, 34, (2009) 3304.
- [8] A. Ancona, F. Röser, K. Rademaker, J. Limpert, S. Nolte, and A. Tünnermann: *Opt. express*, 16, (2008) 8958.
- [9] G. Raciukaitis: *J. Laser Micro Nanoengin.*, 4, (2009) 186.
- [10] S. Kraft, J. Schille, S. Mauersberger, L. Schneider, and U. Loeschner, *Proc. SPIE*, Vol. 11268, (2020) 112681H.
- [11] A. Gillner, J. Finger, P. Gretzki, M. Niessen, T. Barthels, and M. Reininghaus: *J. Laser Micro Nanoengin.*, 14, (2019) 129.
- [12] B. Neuenschwander, B. Jaeggi, M. Zimmermann, V. Markovic, B. Resan, K. Weingarten, R. de Loor, and L. Penning: *J. Laser Appl.*, 28, (2016) 22506.
- [13] G. Raciukaitis: *IEEE J. Select. Topics Quantum Electron.*, 27, (2021) 1.
- [14] B. Neuenschwander, G. F. Bucher, C. Nussbaum, B. Joss, M. Mural, U. W. Hunziker, and P. Schuetz, *Proc. SPIE*, Vol. 7584, (2010) 75840R.
- [15] B. Jaeggi, B. Neuenschwander, M. Zimmermann, L. Penning, R. deLoor, K. Weingarten, and A. Oehler, *Proc. SPIE*, Vol. 8967, (2014) 89670Q.
- [16] J. Finger, B. Bornschlegel, M. Reininghaus, A. Dohrn, M. Nießen, A. Gillner, and R. Poprawe: *Adv. Opt. Technol.*, 7, (2018) 145.
- [17] J. Finger and M. Hesker: *J. Phys. Photonics*, 3, (2021) 21004.
- [18] A. Gillner, P. Gretzki, and L. Büsing, *Proc. SPIE*, Vol. 9740, (2016) 974010.
- [19] T. Barthels and M. Reininghaus, *Proc. SPIE*, Vol. 10744, (2018) 107440B.
- [20] B. Jäggi, L. Canguero, D. Bruneel, J. A. Ramos de Campos, C. Hairaye, and B. Neuenschwander, *Proc. SPIE*, Vol. 10519, (2018) 1051905.
- [21] B. Neuenschwander, T. Kramer, B. Lauer, and B. Jaeggi, *Proc. SPIE*, Vol. 9350, (2015) 93500U.
- [22] N. Hodgson, H. Allegre, A. Starodoumov, and S. Bettencourt: *J. Laser Micro Nanoengin.*, 15, (2020) 236.
- [23] B. Bornschlegel and J. Finger: *J. Laser Micro Nanoengin.*, 14, (2019) 88.
- [24] C. Kerse, H. Kalaycıoğlu, P. Elahi, B. Çetin, D. K. Kesim, Ö. Akçaalan, S. Yavaş, M. D. Aşık, B. Öktem, H. Hoogland, R. Holzwarth, and F. Ö. Ilday: *Nature*, 537, (2016) 84.
- [25] S. M. Remund, M. Gafner, M. V. Chaja, A. Urniezius, S. Butkus, and B. Neuenschwander: *Procedia CIRP*, 94, (2020) 850.
- [26] G. Bonamis, E. Audouard, C. Hönninger, J. Lopez, K. Mishchik, E. Mottay, and I. Manek-Hönninger: *Opt. express*, 28, (2020) 27702.
- [27] X. Wolters, G. Bonamis, K. Mishchick, E. Audouard, C. Hönninger, and E. Mottay: *Procedia Manufacturing*, 36, (2019) 200.
- [28] A. Žemaitis, P. Gečys, M. Barkauskas, G. Račiukaitis, and M. Gedvilas: *Sci. reports*, 9, (2019) 12280.
- [29] A. Žemaitis, M. Gaidys, P. Gečys, M. Barkauskas, and M. Gedvilas: *Opt. express*, 29, (2021) 7641.
- [30] F. Caballero-Lucas, K. Obata, and K. Sugioka: *Int. J. Extrem. Manuf.*, 4, (2022) 15103.
- [31] F. Bauer, A. Michalowski, T. Kiedrowski, and S. Nolte: *Opt. express*, 23, (2015) 1035.
- [32] B. Jäggi, D. J. Förster, R. Weber, and B. Neuenschwander: *Adv. Opt. Technol.*, 7, (2018) 175.
- [33] T. Kramer: *J. Laser Micro Nanoengin.*, 12, (2017) 107.
- [34] B. Bornschlegel, M. Kratz, and J. Finger: *J. Laser Micro Nanoengin.*, 17, (2022) 19.
- [35] D. J. Förster, S. Faas, S. Gröninger, F. Bauer, A. Michalowski, R. Weber, and T. Graf: *Appl. Surf. Sci.*, 440, (2018) 926.
- [36] D. J. Förster, B. Jäggi, A. Michalowski, and B. Neuenschwander: *Materials*, 14, (2021) 3331.
- [37] M. Tsukamoto, T. Kayahara, H. Nakano, M. Hashida, M. Katto, M. Fujita, M. Tanaka, and N. Abe: *J. Phys.: Conf. Ser.*, 59, (2007) 666.
- [38] A. Brenner, B. Bornschlegel, and J. Finger: *J. Laser Micro Nanoengin.*, 14, (2019) 100.
- [39] A. Brenner, B. Bornschlegel, and J. Finger, *Proc. SPIE*, Vol. 10730, (2018) 107300H.

(Received: July 31, 2023, Accepted: January 6, 2024)